Inductive Monitoring of Joint Kinematics: A Study of Canonical vs. Anatomical Tissue Models

Undergraduate Honors Research Thesis

Shanila Reza

Advisor: Asimina Kiourti

The Ohio State University

Department of Electrical and Computer Engineering

Abstract

The ElectroScience Lab has demonstrated the feasibility to monitor joint flexion and rotation using wearable electrically small loop antennas. Currently, the research uses canonical (cylindrical) tissue models. The objective of this research is to transition cylindrical to anatomical models which will be used to refine the sensors. The anatomical details are varied for diverse individuals and then sensors are optimized for each individual to aid in finding calibration techniques for real life operation. To meet the objectives mentioned, canonical tissue models are replaced with anatomical ones, as readily available in libraries tied to electromagnetic solvers. Then the sensor design is modified to fit the anatomical geometries and simulations are run. The sensor design is optimized for each geometry, and a methodology is created to optimize sensor design for different body parts. Analysis of the results will help find ways to calibrate the sensor in real world conditions.

Acknowledgements

I would like to the thank the Wearable and Implantable Technologies group. I would like to thank Dr. Asimina Kiourti and Vigyanshu Mishra who did an amazing job of mentoring and supporting me during this thesis.

Table of Contents

List of Tables

List of Figures

Chapter 1: Introduction

1.1: Need for Motion Capture and Limitations in the State-of-the –Art

Motion capturing sensors are necessary for applications such as accurately diagnosing sports injuries and monitoring kinematics during physical therapy. Current techniques commonly used have limitations which are summarized in Table 1. On-body-retro-reflective markers tracked by infrared are "gold standard" for monitoring kinematics but are restricted to lab environments. Other methods such as markless cameras are limited by line-of-sight and laboratory environments [3],[4]. Inertial Measurement Units (IMUs) are limited by their obtrusive nature, and they suffer from integration drift [5-7]. Time-of-flight sensors are limited by line of sight [8]. Also, bending sensors are used for monitoring kinematics, but they obstruct natural movement and only work for a limited number of cycles [9] [10].

Table 1: Comparison of Approaches for Monitoring Joint Flexion

	Camera-based	IMUs	Time-of-Flight	Bending Sensors	Proposed
Works in real-world settings	No (-)	Yes (+)	Yes (+)	Yes (+)	Yes (+)
Seamless	Yes (+)	No (-)	No (-)	Yes (+)	Yes (+)
Insensitive to Line-of-Sight	No (-)	Yes (+)	No (-)	Yes (+)	Yes (+)
Allows natural motion	Yes (+)	Yes (+)	Yes (+)	No (-)	Yes (+)
Reliable vs. time	Yes (+)	No (-)	Yes (+)	No (-)	Yes (+)
3D motion capture	Yes (+)	Yes (+)	Yes (+)	Flexion only	Flexion only

The proposed research will advance the monitoring of joint kinematics by taking steps towards using electrically small loop antennas to monitor joint flexion and rotation in real-world environments by transitioning to demonstrating the sensors on diverse anatomical models in

simulations using CST, an electromagnetic solver. Advancing the monitoring of joint kinematics using electromagnetic sensors that overcome the state-of-the-art limitations outlined in Table 1, will bring more opportunities for applications as diverse as gestural interaction, rehabilitation, and sports [1]. Proof-of-concept results demonstrate feasibility but are limited to simplified geometries that emulate the human limb as a cylinder. Anatomical details have not been considered, and inter-subject anatomical differences (geometry, size, etc.) have not been explored to date. This proposed research aims to overcome all of these limitations. The transition of using anatomical models for diverse individuals, and then finding a way to calibrate the sensors in real world settings will pave the way for monitoring joint kinematics without limitations of integration drift, lab environments, requirement of line-of-sight, and obstruction of natural movement.

1.2: Case Study: Anterior Cruciate Ligament Reconstruction

Advancing monitoring of joint kinematics could pave the way for improved treatment for anterior cruciate ligament (ACL) injuries. It is important to improve the treatment of anterior cruciate ligament (ACL) injuries because ACL injuries cause joint effusion, reduced functional performance, muscle weakness, and altered movement [11,12]. Additionally improper monitoring can increase the risk of a second ACL injury [14].

Basics of ACL Reconstruction: ACL Reconstruction (ACLR) aims to restore the ACL. 65% of people who get ACL injuries get ACLR [13]. After ACLR, cartilage degeneration and early progression of osteoarthritis is indicated by clinical studies. Osteoarthritis may be caused by improper restoration of normal neuromuscular function and kinematics. Other common symptoms after ACLR include impaired function, joint effusion, lack of normal joint range of

motion, and muscle weakness. Less than 50% of athletes return to sports within a year of getting ACLR [11].

The success rate of ACLR and postsurgical rehabilitation is between 43% - 93%, and after ACLR, biomechanical and neuromuscular channel patterns deviate from normal for up to two years [14]. Increased proper monitoring of progress after ACLR may help increase proper restoration [3]. ACL rehabilitation currently does not involve monitoring daily activities. The monitoring of daily activities is crucial to preventing decreased knee extensor weakness which is caused by abnormal movements during daily activities [11].

Motion capturing sensors such as the ones explored and refined in this thesis, can provide daily monitoring to people after ACLR and lead to higher success rates of postsurgical rehabilitation. The proposed motion capturing sensors can find abnormal movements during daily activities which would prevent knee extensor weakness. Additionally, properly monitoring daily activities could help restoration of normal neuromuscular function and kinematics which would decrease risk for osteoarthritis [11].

Gender differences before ACL injury: There are gender differences for uninjured athletes. Females are several times more likely to sustain an initial ACL injury when compared to males who are equally active. Larger ground reaction forces, altered peak hip and knee flexion angles, increased frontal plane of motion of the hips and knee were demonstrated by uninjured females in comparison to uninjured males during athletic tasks [14]. In a study, during weight and non-weight bearing activities, healthy women showed reduced dynamic knee stiffness even though lower extremity muscle activity is higher for women. The findings from the study show there are sex-specific differences in neuromuscular strategies of risk of primary ACL injury [14]. Also, dynamic knee valgus, ankle eversion, and peak hip adduction occurred earlier in women when

compared to men during a drop-jump landing task [4]. Another factor in initial ACL injury risk for young females is thigh muscle strength.

Gender differences after ACLR: If the coil-based wearable sensors explored in this thesis are used for monitoring kinematics, different tasks should be tested based on gender. Responses to physical therapy are different for males and females.

Responses to surgery and physical therapy are different for females and male noncopers. Non-copers are patients who have knee instability and dysfunction [15]. A study was conducted with 40 noncopers who were split up to only do perturbation group or strength training. The study investigated the differences between men and women on knee angle tibial position during unilateral standing tasks before and after ACLR, and the effects of perturbation training. No statistically significant differences were found between the perturbation group and strength training group. However, the study found that gender must be considered for non-copers following rehabilitation surgery in neuromuscular behaviors. The study suggests there are gender-specific kinematic responses to preoperative intervention and ACL reconstruction. Unique unilateral standing strategies were present for males and females. Within the group of non-copers, early after injury and 6 months after surgery, only females showed posterior tibial positioning. Females also were more responsive to preoperative physical therapy. This is due to posterior tibial positioning and knee angle asymmetry of the involved limb resolving before the surgery [15].

Second ACL Injury Risk: The risk of second ACL injury is between 6% and 30% and improving joint kinematics monitoring to more accurately determine when it is safe to send people back to daily activities and sports could lower the risk of second ACL injury [14]. Neuromuscular control deficiencies are the only known predictive factor that can be modified. A way to reduce

reinjury is to target interventions using the motion capturing sensors that are explored in this thesis to improve neuromuscular control [14].

Chapter 2: Sensor Operation

2.1: Operating Principle

The sensor consists of two wrap-around coils around a limb. The transmitting coil is placed above the joint, and the receiving coil is placed below the joint. In Figure 1, the sensor is shown where the Rx coil is the receiving coil and the Tx coil is the transmitting coil.

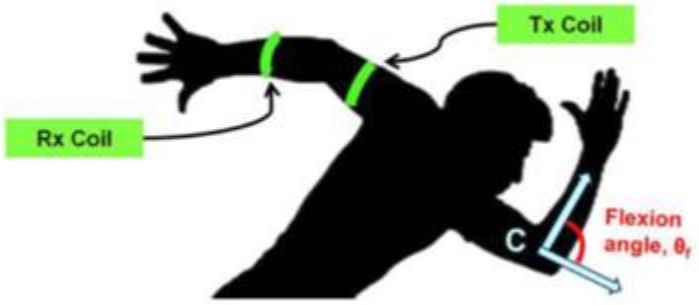

Figure 1: Wrap Around Coils for Joint Flexion [1]

Faraday's Law of Induction explains how the flexion angle, θ_f, is found. A time-varying current flows through the transmitting coil generating a time-varying magnetic flux density in the receiving coil. According to Faraday's Law of Induction, a voltage is induced on the receiving coil. How the voltage induced on the receiving coil, V_{Rx}, is found is shown below, where B_{Tx} is the magnetic flux density, and $\hat{n}_{Rx}$ is the normal unit area vector of the receiving coil [1].

$$V_{Rx} = -\frac{d}{dt}\iint \boldsymbol{B_{Tx}}.\widehat{\boldsymbol{n_{Rx}}}\, ds \tag{1}$$

The flexion angle can be correlated with the induced voltage on the receiving coil, so V_{Rx}, is a function of the flexion angle. The transmission coefficient, $|S_{21}|$, is also a function of the flexion angle [1]. In Figure 2a below, transmission coefficients versus frequency for different flexion angles are shown. Figure 2b shows transmission coefficient versus flexion angle at a frequency of 34 MHz. The plots in Figure 2 are the results from simulations using cylindrical models. In this thesis, the research will transition and similar results will be produced using anatomical models.

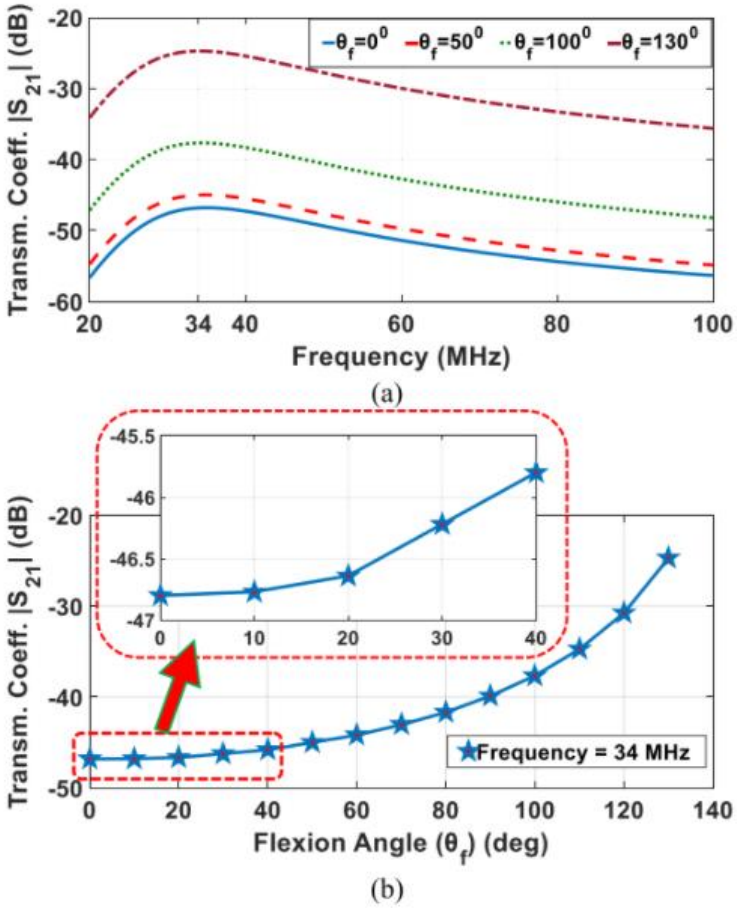

Figure 2: Proof-of-concept for 34 MHz Resonant Coils on Cylindrical Models: (a) $|S_{21}|$ as a Function of Frequency at Different Flexion Angles, and (b) $|S_{21}|$ as a Function of Flexion Angle [1]

2.2 Limitations of Prior Work

A limitation of previous research was the use of only canonical models to demonstrate the feasibility of electrically small loop antennas for joint kinematics monitoring.

Previous proof-of-concept results are limited to cylindrical models which simplify the human limb because cylindrical models do not consider anatomical details. In Figure 3, the cylindrical model during an experimental set-up is shown.

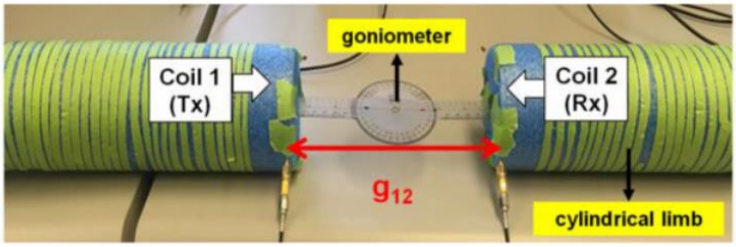

Figure 3: Cylindrical Model with Sensors [1]

The proposed research will bring the sensors a step closer to being used in the real-world by advancing from using cylindrical models to anatomical models. The proposed research uses BioModels in CST which have anatomical details not previously used. Additionally, two different BioModels will be used to observe the sensors on individuals with anatomical differences.

Testing the sensors on anatomical models will also give insight into calibration of the sensor in the real world. No calibration was necessary for sensors tested on cylindrical models,

but calibration will be needed to account for differences between each individual. Conducting simulations on different human models of different sizes will help find what $|S_{21}|$ parameter corresponds with each angle when the size of the limb changes. Additionally, conducting simulations on diverse models will give insight into how to calibrate the gap(g_{12}) parameter between the coils.

Chapter 3: Modeling Using Voxel Models in CST

3.1 CST Basics

Meshing Type: CST electromagnetic solver was used to simulate different flexion angles on diverse anatomical models. Specifically, the voxel posable BioModels Laura and Gustav were used in CST, as will be described in detail in Section 3.2.

First, the type of meshing was determined. Hexahedral meshing uses the Finite Integration Method with the Perfect Boundary Approximation. For this type of meshing, mapping is done to a hexagonal mesh. Perfect Boundary Approximation maps from the continuous to discrete mesh [16]. Tetrahedral meshing uses Finite Integration Method only and uses tetrahedrons which consist of triangles for meshing [16]. Hexahedral meshing was used because hexahedral meshing is compatible with voxel models. Tetrahedral meshing is better suited for simulating the sensor because tetrahedral meshing works well for thin wires like the 0.0254 cm wires used in real life. However, tetrahedral meshing is not compatible with CST BioModel voxel models.

Time or Frequency Domain: Then the decision between time domain or frequency domain was made. It is noted that time domain is not ideal for the electrically small loop antennas under

consideration because time domain is recommended for thicker wires. Nevertheless, time domain was used because pairing frequency domain with hexahedral meshing results in lossy material being treated as a perfect electric conductor (PEC). CST recommended using tetrahedral meshing instead, but tetrahedral meshing is not compatible with voxel data, so the only combination of meshing type and domain compatible with simulating the sensor on voxel BioModels is hexahedral meshing and time domain.

Then the global meshing properties were adjusted to make sure the discrete ports and capacitors were accurately represented. The global meshing properties were adjusted to create a finer mesh to resolve the issue of a single point representing discrete ports and capacitors. Additionally, using a finer mesh allowed for the use of thinner wires. The methodology for selecting the global meshing properties and wire diameter is described in more detail in Chapter 4.

3.2 Posable Tissue-Emulating Models in CST

The objective of the proposed research was to transition from cylindrical models to diverse anatomical models. The anatomical models used were the Posable BioModels available in CST. The only posable models are Laura, Gustav, and Hugo. Selecting Laura and Gustav allowed for opportunity to run simulations on two genders. In the future, running simulations on Hugo is also an option to obtain results on a model of a different size.

Images of Gustav and Laura are shown below in Figures 4 and 5. Gustav is based on a 38-year-old male who is 176 cm tall and weighs 69 kg. Laura is based on a 43-year-old female who is 163 cm and 51 kg [17].

Figure 4: Laura BioModel [17]

Figure 5: Gustav BioModel [17]

Chapter 4: Sensor Design Methodology

4.1 Methodology for Finding Optimal Wire Diameter to Use with Hexahedral Meshing in Time Domain

Global Mesh Properties: To find the optimal wire diameter for the sensors, first the global meshing properties were adjusted. The global meshing properties were adjusted first because global meshing properties will determine the precision of the mesh, which is responsible for how the solids are discretized which effects how thin the wire can be. Global meshing properties were adjusted to be 15 cells per wavelength near the model, 2 cells per wavelength far from the model, 45 cells per max model box edge, 2 cells per max model box edge, and 20 fracton of maximum cell near to model for the minimum cell which resulted in the specifications shown in Figure 6.

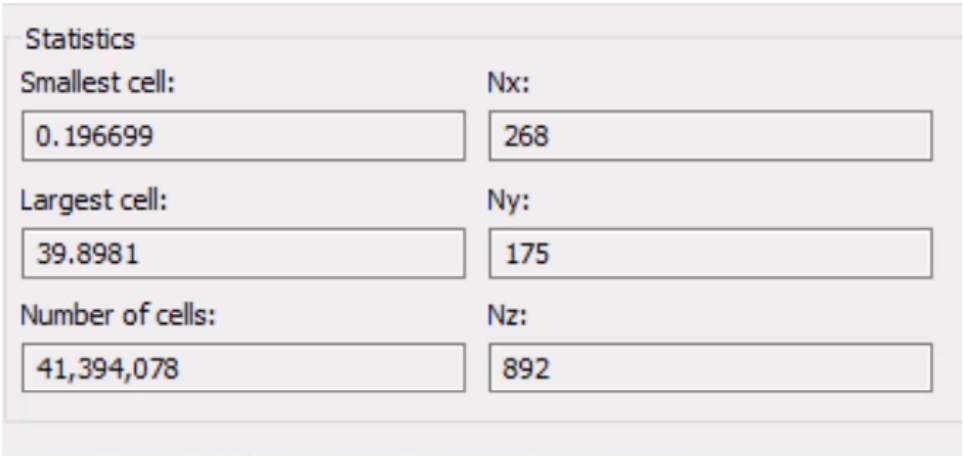

Figure 6: Specifications of Global Mesh Properties

Wire Diameter: First, a wire diameter of 0.0254 cm was tried which is the diameter of the wire used in real life, and the wire diameter used in the CST simulations using the cylindrical models.

A wire diameter of 0.0254cm did not work because the domain was changed from frequency domain to time domain, and time domain is more compatible with thicker wires. Then a 1.0 cm diameter was tried, and the simulation ran. Then simulations were ran to find the smallest wire diameter that worked in the time domain with hexahedral meshing. Table 2 outlines which wire diameters were tried and which ones worked. The method used was averaging a wire diameter that works and a wire diameter that does not work and then trying that value for the wire diameter. 0.05cm was found to be the optimal wire diameter to use in the time domain with hexahedral meshing with the previously described global meshing properties.

Table 2: Method for Finding Optimal Wire Diameter to Use in Time Domain with Hexahedral Meshing

Wire Diameter (cm)	Did it work in the Time Domain with Hexahedral Meshing	Logic to testing specific wire diameter
0.0254	No	Wire diameter used in real life and in simulations with cylindrical model in frequency domain with tetrahedral meshing
0.5	Yes	Trying to find a wire diameter >0.0254 that works
0.1	Yes	Trying to find 0.0254 cm< optimal wire diameter < 0.5 cm
0.05	Yes	Trying to find 0.0254 cm< optimal wire diameter < 0.1 cm. Divided 0.1cm by 2
0.025	No	Trying to find 0.0254 cm< optimal wire diameter < 0.05 cm. Divided 0.05cm by 2
0.0375	No	Trying to find 0.025 cm< optimal wire diameter < 0.05

		cm. Took average of 0.025 (does not work) and 0.05 (works)
0.046875	No	Trying to find 0.0375 cm< optimal wire diameter < 0.05 cm. Took average of 0.0375 cm (does not work) and 0.05 cm (works)

Decisions on time and CPU usage limits: The decided upon wire diameter was 0.05cm. This is the smallest wire diameter worked with the settings previously determined. A smaller wire diameter would potentially work if the global meshing properties were changed to create a finer mesh; however, time is a tradeoff when creating a finer mesh. The finer the mesh becomes, the longer the simulation takes to finish. The simulation was left running at finer meshes for approximately 15 hours, and they never finished. Additionally, excessively fine meshing causes CST to crash after a point and uses above 90% CPU. It was determined simulations that run over 15 hours and above 90% CPU usage was too long of a time and too great CPU usage for a simulation.

4.2 Methodology to Modify Sensor Design for Diverse Individuals

First, a methodology was determined to fit the coils around the limbs of the BioModels to keep an accurate flexion angle and gap between the coils. The flexion angle is the angle the joint is bent and is shown in Figure 1 above.

Simulations were ran on the BioModel Gustav to test a 50-degree flexion angle. The following steps describe how to set up the simulation for a flexion angle of 50 degrees at the elbow on Gustav.

1. Set up the Rx and Tx coil as you would for a cylindrical model.
    a. Have the following changeable parameters for:
        i. The Rx coil
        ii. The Tx coil
        iii. The gap between the coils
        iv. Theta
        v. Wire Diameter
2. Import posable BioModel Gustav
3. Adjust the diameter of the coils, so the Tx coil fits closely to the upper arm and the Rx coil fits closely to the forearm without going inside the tissue of the BioModel.
4. Make adjustments to the posable model by deleting the Posable BioModel Gustav and reimporting the Posable BioModel Gustav and posing Gustav using the Poser tool so the flexion angle of the posable model is closer to the desired angle flexion angle the coils are at.
5. Repeat steps 3 and 4 to get the flexion angle of the BioModel closest to the desired angle and to have the coils fit to the closest 0.1cm diameter to the BioModel.

The diameter for the Rx coil was determined to be 5cm, and the diameter for the Tx coil was determined to be 5cm for Gustav. The gap g_{12} is the gap between the Rx and Tx coils and controls the range of flexion angles that can be measured because the smaller the gap the closer the coils are to touching, resulting in coils touching when flexion angles are larger. Also, decreasing the gap causes $|S_{21}|$ to increase non-linearly which results in lower power requirements because the magnetic field and gap between coils have an inverse relationship [1].

The gap used for simulating the electrically small loop antennas on the BioModel Gustav was 10cm, the same gap as the cylindrical model.

Steps 1-5 were used to complete the simulation for Gustav's arm with a 50-degree flexion angle. For testing other flexion angles for Gustav, all settings were kept the same except the l_elbow, the label for the elbow joint in CST Poser which is the joint adjusted to position the BioModel to the desired flexion angle. There are three directions for the l_elbow joint which can be adjusted. The U direction is the adjustment of flexing your forearm towards your bicep. The only adjustment when changing flexion angles was adjusting the l_elbow joint in the U direction. The l_elbow joint in the U direction of the Posable BioModel Gustav was set to the flexion angle * -1 + 3 (ex: A flexion angle of 50 degrees would result in the l_elbow angle in the U direction to be –47 degrees) because the resulting position fit in the coils at the desired flexion angle every time. In Figure 7. the left arm of Posable BioModel Gustav with a flexion angle of 50 degrees at the elbow joint is shown with fitted wearable electrically small loop antennas. For Gustav's left arm, angles 10, 20, 30, 40, 50, 60, 70, and 80 degrees were simulated. The range of angles for Gustav's arm is more limited than the range of angles for the cylindrical model (0-130 degrees) because of limitations of CST Poser which is used for posing the BioModel. L_elbow has limitations for what angle it can be set to. To prevent the BioModel from being in an unnatural position of bending backwards at the elbow, the l_elbow joint is limited to only flex towards the bicep. Testing an angle of 0 degrees would require the l_elbow angle in the U direction to be –3 degrees, and negative angles are not possible in the U direction because the forearm would be bending away from the bicep which is unnatural. Also, flexion angles above 80 degrees could not be tested because the Tx and Rx coils were too big on the Gustav model resulting in the coils

overlapping. Adjusting the gap (g_{12}) could resolve the issue of the coils overlapping at higher flexion angles.

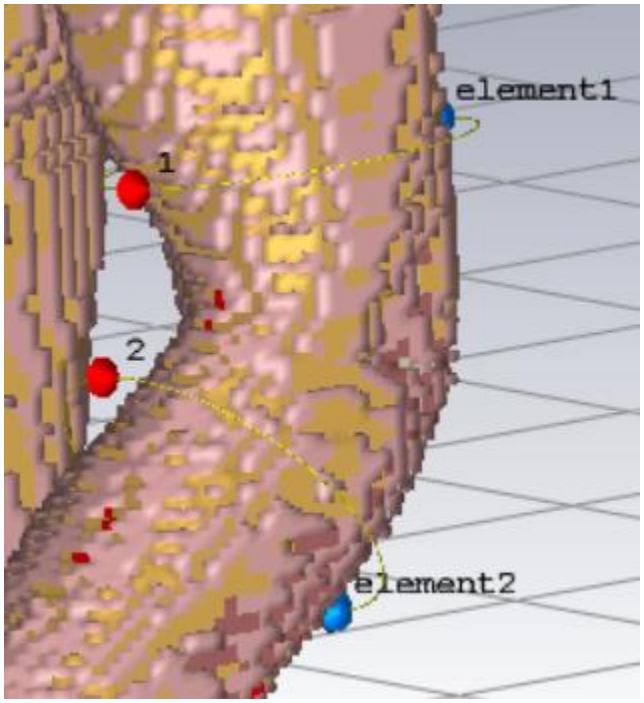

Figure 7: CST Anatomical Model (Laura) with Adjusted Sensors on Arm

For the Posable BioModel Laura, Steps 1 – 5 were followed to get the flexion angle of the BioModel closest to the desired flexion angle and to have the coils fit to the closest 0.1cm diameter to the BioModel. The diameter of the Rx coil was determined to be 4.8 cm and the diameter of the Tx coil was determined to be 5.0 cm. The same flexion angles (10, 20, 30, 40, 50, 60, 70, and 80) were simulated. 0 degrees could have been simulated for Laura but was not simulated because there was no equivalent simulation from Gustav. All settings were kept the same for all flexion angles other than the l_elbow angle in the U direction which was changed to the flexion angle * –1 - 9 (ex. A flexion angle of 50 degrees would result in the l_elbow joint U direction angle to be -59 degrees). The range of flexion angles for Laura are limited for the same reason as the flexion angles for Gustav are.

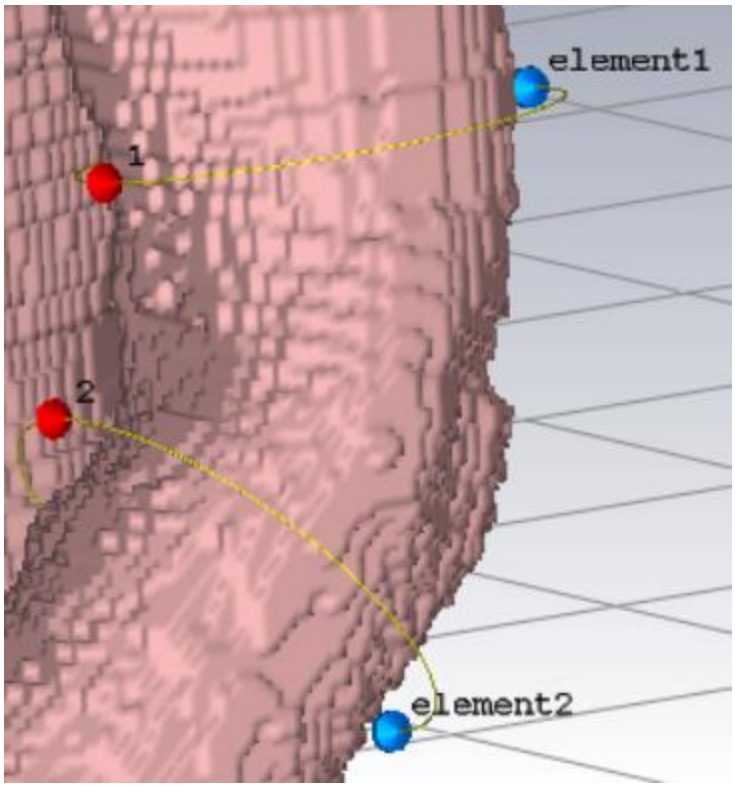

Figure 8: CST Anatomical Model (Gustav) with Adjusted Sensors on Arm

Chapter 5: Results and Discussion

The electrically small loop antennas for monitoring joint kinematics were successfully transitioned from being demonstrated on canonical (cylindrical) tissue models to anatomical models. The sensors were refined for two anatomical models, Laura and Gustav, voxel BioModels found in CST. The sensors were refined for Laura's left arm and Gustav's left arm and the results show flexion angle is still correlated with the transmission coefficient $|S_{21}|$, so the flexion angle can be successfully found on an anatomical model by measuring the $|S_{21}|$ parameter. The selected operation frequency was the same as it was for the cylindrical models which is 34 MHz because this frequency is in inductive mode and allows for lower power

requirements, a desirable flexion angle resolution, and provides enough robustness to work with diverse individuals [1]. Figure 9 show the transmission coefficient vs flexion angles for Gustav and Laura. Similarly, to simulations run on cylindrical models, a one-to-one ratio is shown between the transmission coefficient and flexion angles for both Gustav and Laura when the transmission coefficient is taken at 34 MHz. Since there is one transmission coefficient for every flexion angle for Gustav and Laura, it is feasible to use electrically small wearable antennas to measure flexion angle on diverse anatomical models.

In Figure 9, the transmission coefficients that correspond with each flexion angle is different for Gustav and Laura because the sizes and tissue composition of both models are different. The radii of the coils for Gustav were 5.0cm for the Rx coil and 5.0cm for the Tx oil. The radii of the coils for Laura were 5.0cm for the Rx coil and 4.8cm for the Tx coil. Laura has a coil that is smaller and consistently has smaller transmission coefficients for each flexion angle than Gustav. The results in this thesis show there is a direct relationship between coil radii and transmission coefficients. Further research will need to be done to gain more data to be able to create algorithms that can accurately predict what the corresponding transmission coefficient for each angle will be for different coil radii.

Figure 10 shows the transmission coefficient plotted against the flexion angle and the transmission coefficient is taken at the optimal or resonance frequency of each sensor. The transmission coefficients values for both Gustav and Laura are much closer in value for each flexion angle when compared to the transmission coefficients taken at 34 MHz. In the future, taking transmission coefficients at the optimal frequency for each sensor may be a good option.

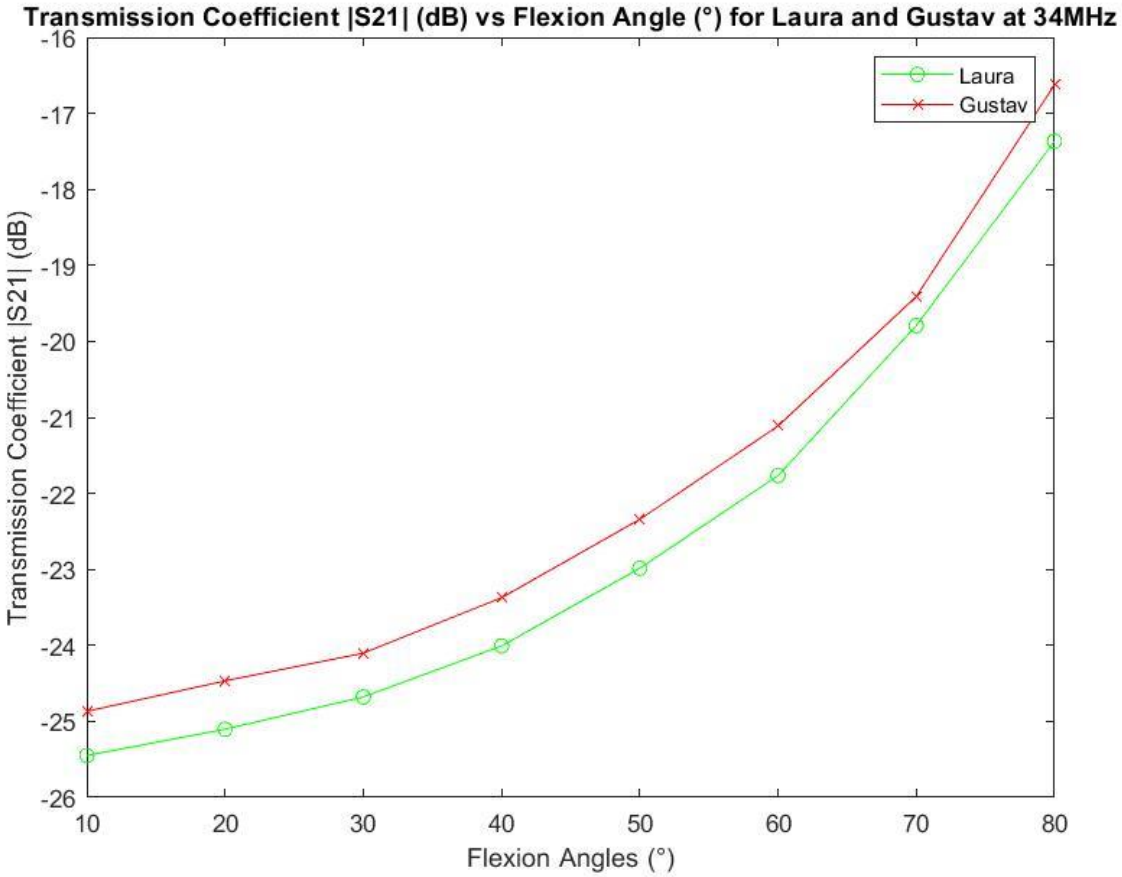

Figure 9: Transmission Coefficient $|S_{21}|$ (dB) vs Flexion Angle (°) for Laura and Gustav at 34MHz

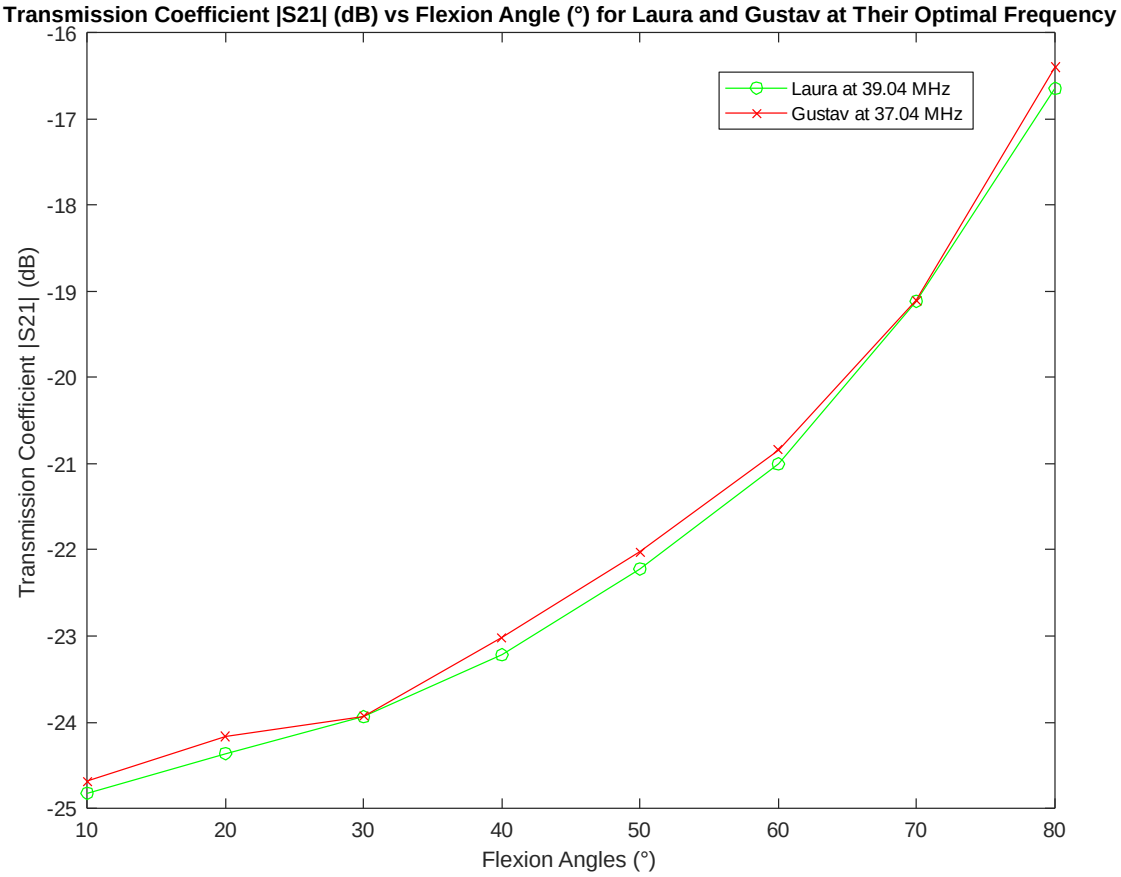

Figure 10: Transmission Coefficient $|S_{21}|$ (dB) vs Flexion Angle (°) for Laura and Gustav at Their Optimal Frequency

A potential way of calibrating the sensors in real life is to insert the radii of the individual's arms when the coils are placed at a 10cm, 15cm, and 20cm gap. With the radii of the individual arms, and potential gap lengths, a gap can be selected that is large enough to have the desired range and resolution of flexion angles and small enough to have desirable low power requirements. Then, there should be an algorithm that inputs gap and coil radii and outputs which transmission coefficient should correspond with each flexion angle. So far trends have been and

transmission coefficient values that correspond with different flexion angles have been found for two different CST BioModel arms. The next step is to create an algorithm which uses the mathematical relationship between the gap and radii and the resulting transmission coefficient for each flexion angle. Once a gap and radii are selected, the output of the algorithm should be similar to Figure 9. Then transmission coefficients or other measurements that have a one-to-one relationship with the flexion angles, such as the induced voltage on the transmitting coil, should be measured. Using the data from the plot outputted by the proposed algorithm and the measurement of the transmission coefficient or induced voltage on the transmitting coil, the angle should be able to be determined.

The specifications that were used for the simulations for Gustav and Laura that resulted in the results shown in Figures 9, 11, 13, 14, 15 are shown in Table 3.

Table 3: Summary of Specifications and Suggestions for Electrically Small Loop Antennas on Diverse Anatomical Models

Parameter	Gustav BioModel (cm)	Laura BioModels (cm)
Rx coil radius	5	5
Tx coil radius	5	4.8
Gap (g_{12})	10	10
Resonance Frequency (MHz)	~37.04	~39.04
Measurable Flexion Angle Range	10° -80°	0° -80°
Suggestions	Increase coil gap	Increase coil gap

Details on how to use CST Voxel Models to recreate results or to further explore how to optimize the motion capturing sensors is in Appendix A.

The transmission coefficients also increase as angle increases which was also shown in previous research using cylindrical models [1]. Figures 11 and 12 which are the results of transmission coefficient vs. frequency for Gustav and Laura at 10°, 50°, 80°, follow similar trends to Figure 13 which is the results from a simulation on a cylindrical model. A difference between all the results is different resonance frequencies. The resonance frequency of the cylindrical models is at the determined optimal frequency of 34 MHz. The resonance frequency for Gustav is approximately 37.04 MHz, and the resonance frequency for Laura is approximately 39.04MHz. No adjustments were made to make the resonance frequency for the simulations with the BioModels the desirable 34MHz. In the future, different capacitors other that a 95pF capacitor could be used to make the coils resonant at 34MHz.

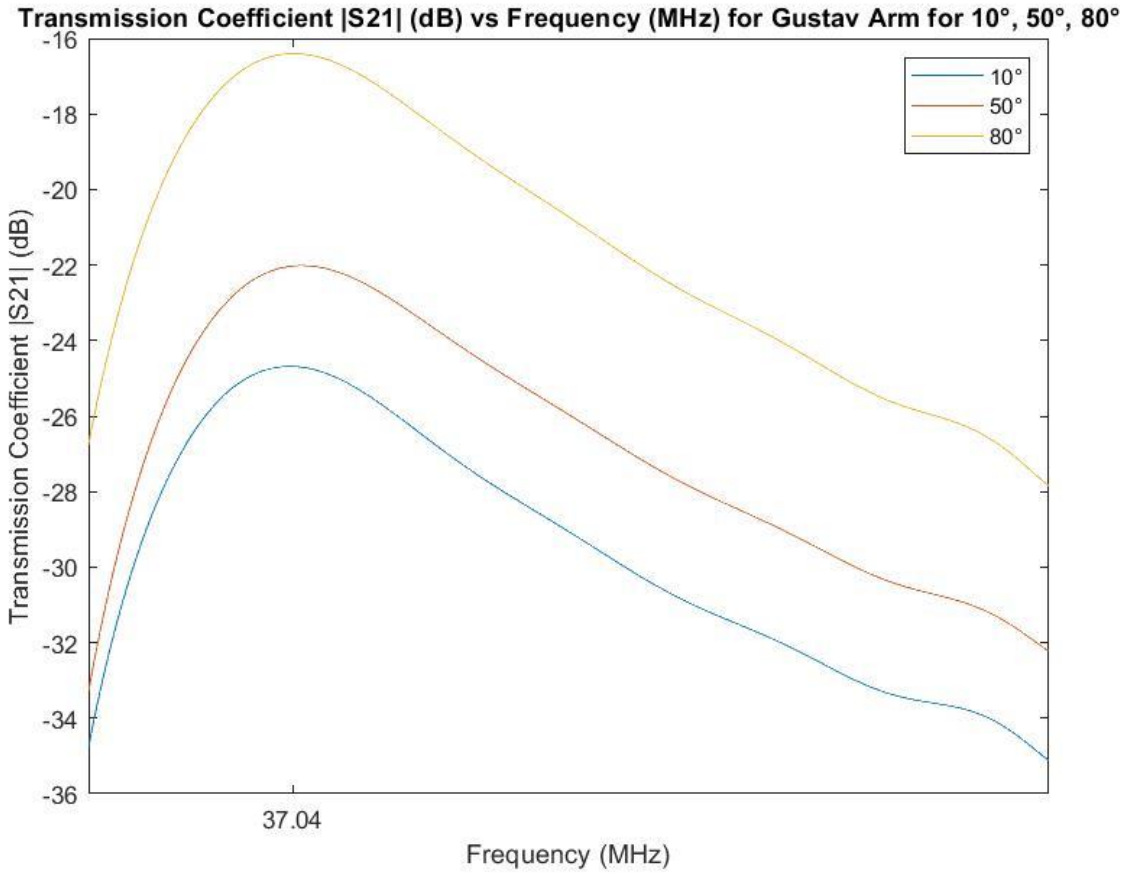

Figure 11: Transmission Coefficient $|S_{21}|$ (dB) vs Frequency (MHz) for Gustav Arm for 10°,

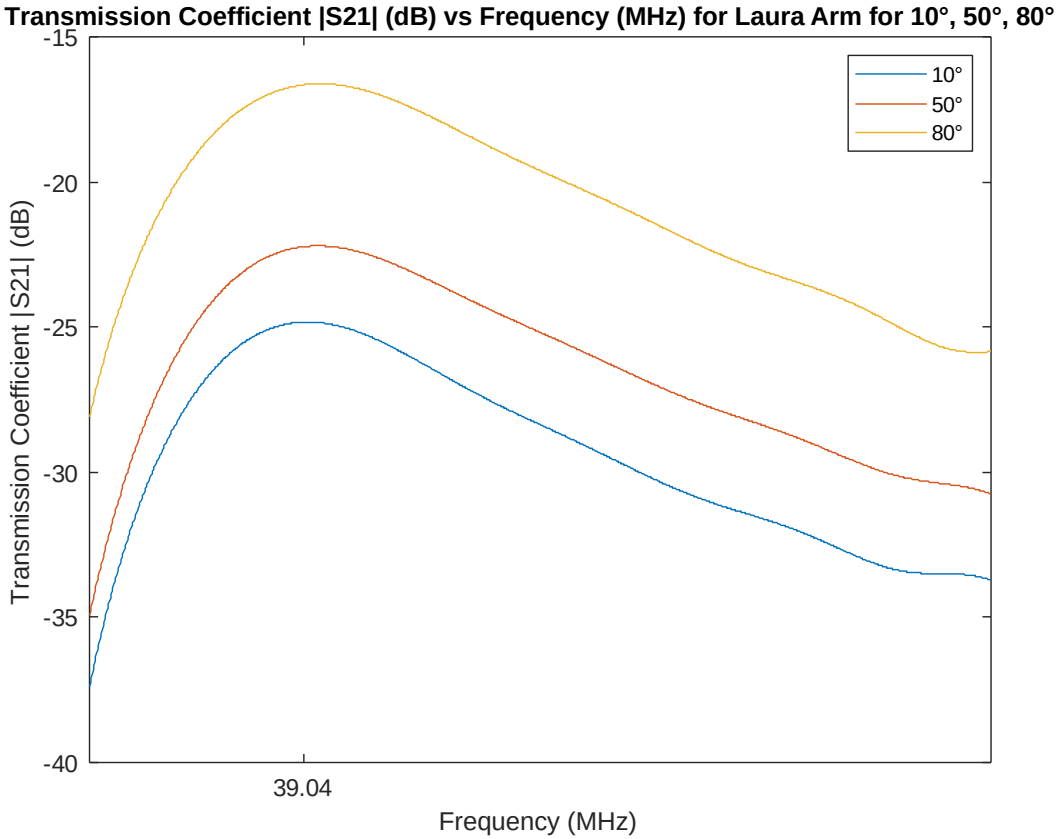

50°, 8

Figure 12: Transmission Coefficient $|S_{21}|$ (dB) vs Frequency (MHz) for Laura Arm for 10°, 50°, 80°

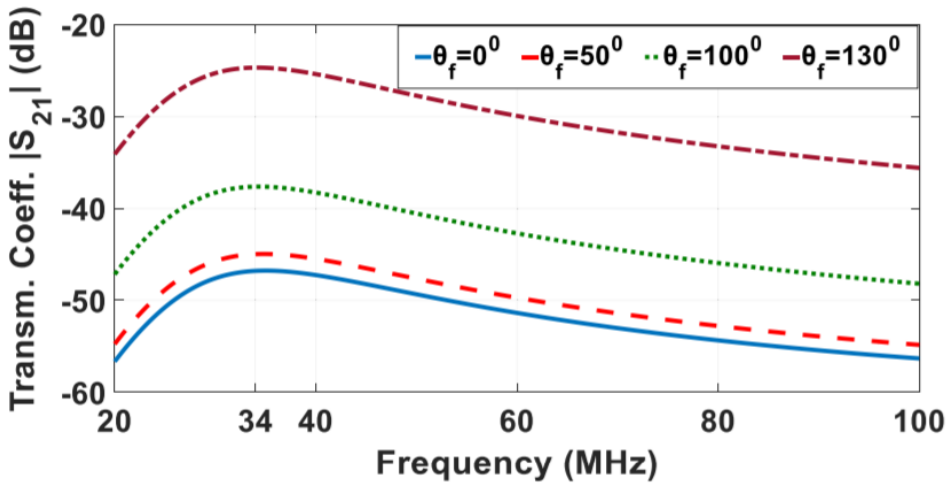

Figure 13: Transmission Coefficient $|S_{21}|$ (dB) vs Frequency (MHz) for Cylindrical Model [1]

Figure 14 shows the transmission coefficient versus frequency for Gustav and Figure 16 shows the transmission coefficient versus frequency for Laura for all angles simulated. Both figures show at a frequency of 34MHz, there is only one transmission coefficient for each angle. The same is shown when considering the resonance frequency of 37.04M Hz for Gustav and resonance frequency of 39.04MHz for Laura. However, at 41.76 MHz, both 20° and 30° have the same transmission coefficient of –24.44 dB for Gustav which is shown in Figure 15. The motion capturing sensors must have a one-to-one relationship between transmission coefficients and flexion angles. Results from simulations with anatomical models show there is still a one-to-one relationship between the transmission coefficient and flexion angle at the optimal frequency of 34Mhz and the resonance frequencies of ~37.04MHz for Gustav and ~39.04 MHz for Laura. However, if you go ~7.76MHz above the optimal frequency of 34MHz and ~4.72 MHz the resonance frequency for Gustav, the one-to-one relationship between the transmission coefficient and the flexion angle is lost. A potential reason the one-to-one relationship may have been lost is because the coils were not fitted perfectly because the arm is not cylindrical, but the coil is cylindrical.

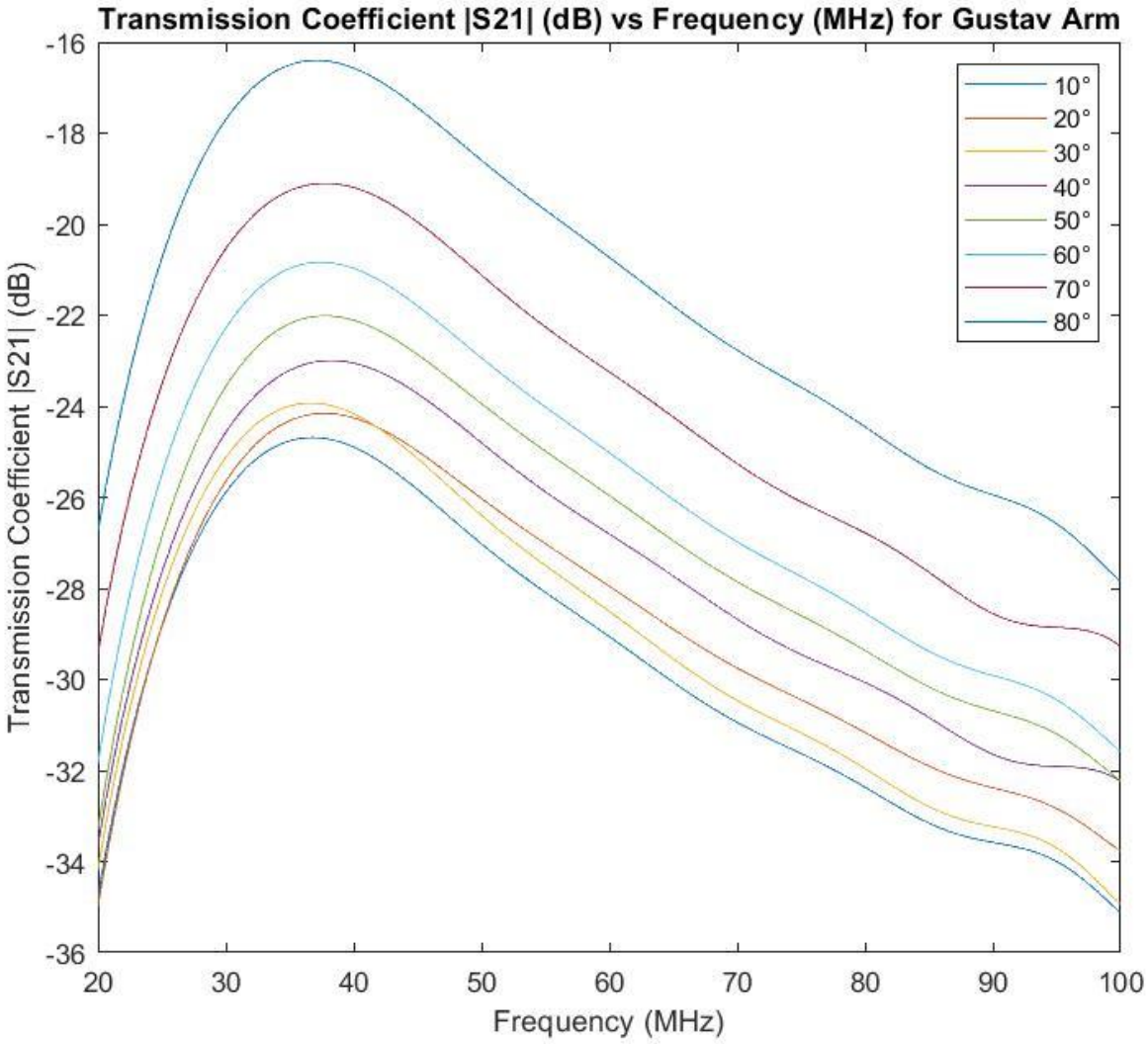

Figure 14: Transmission Coefficient $|S_{21}|$ (dB) vs Frequency (MHz) for Gustav Arm

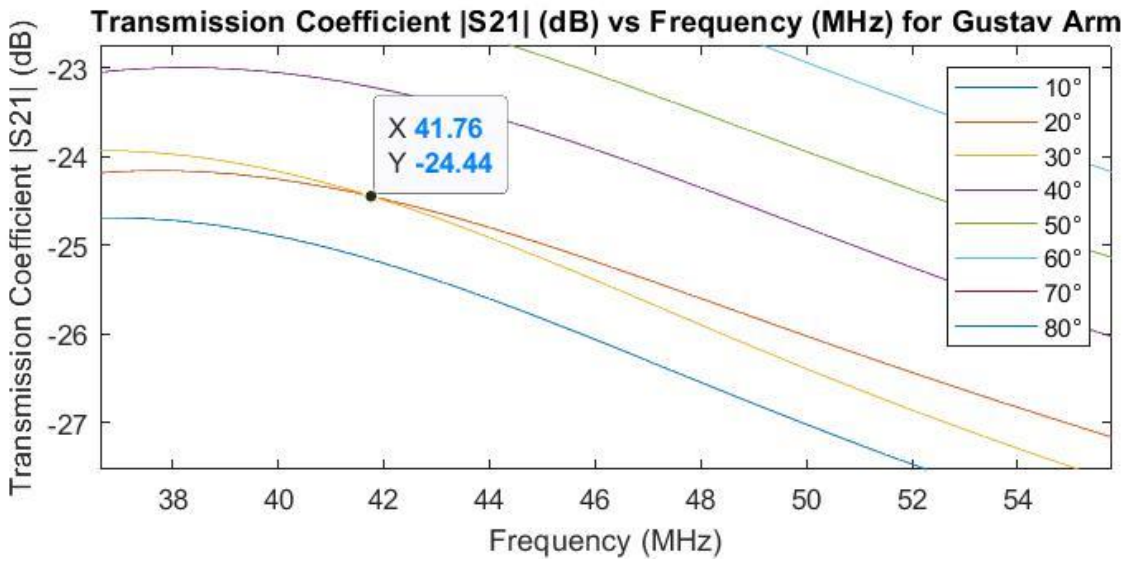

Figure 15: Transmission Coefficient $|S_{21}|$ (dB) vs Frequency (MHz) for Gustav Arm Zoom-In

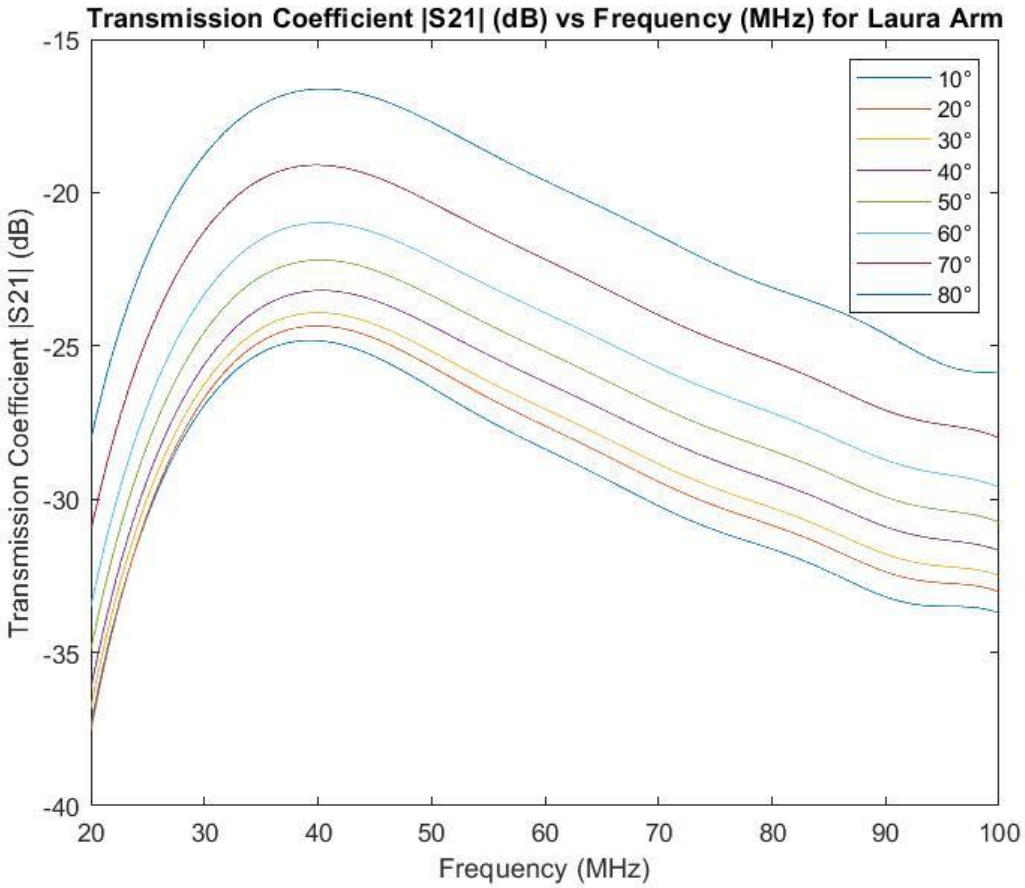

Figure 16: Transmission Coefficient $|S_{21}|$ (dB) vs Frequency (MHz) for Laura Arm

Chapter 6: Conclusion

The feasibility to successfully monitor joint kinematics using electrically small loop antenna was shown using anatomical models. The research on monitoring kinematics with motion capturing sensors was successfully transitioned from canonical (cylindrical models) to diverse anatomical models. Posable BioModels available in CST, Gustav and Laura, were used for the first time to demonstrate the motion capturing sensors. When taking transmission coefficient measurements at the optimal frequency or 34MHz, there is a one-to-one relationship between transmission coefficient and flexion angle which demonstrates it is feasible to obtain the flexion angle from transmission coefficient measurements. There is also a one-to-one relationship between transmission coefficients and flexion angles when transmission coefficients are taken at the resonant frequencies for both models, and the transmission coefficients for Gustav and Laura are closer in value as seen in Figure 10, when the transmission coefficient is taken at each sensor's optimal frequency. The only time there is not a one-to-on ratio between the transmission coefficient and flexion angles is at the frequency of 41.76 MHz for Gustav at 20° and 30°.

Chapter 7: Future Work

The suggestions row in Table 3 addresses limitation that could be resolved in the future which is adjustment of the gap between the coils. A larger coil gap would allow for a larger range of angle and higher angle resolution. Additionally, running more simulations with different coil gaps will give more insight into how to calibrate the coil gap in real life. Also, in the future, determining the value of the lumped capacitor for different individuals will be necessary if the optimal frequency of 34 MHz wants to be achieved.

In the future transitioning to using a program that will allow for coils that are more closely fitted to the arms and coils that are not more cylindrical in shape will give more realistic results. No options to fit the coils to BioModels used were found because voxel BioModel limbs are made up of many cubes rather than shapes for the limb that a coil can fit around. A potential route is to use the CAD BioModels provided by CST. They should be available with the CST BioModel package, but do not seem to be available. Due to time constraints, the option of the CAD BioModel model could not be further explored, but utilizing CAD BioModels can potentially provide more realistic results because using CAD models would overcome the limitations of voxel models, such as not being able to fit the coils around the anatomical model, having to use hexahedral meshing with the time domain when tetrahedral meshing with frequency domain is more ideal and allows for the use of wires that are thinner and closer in diameter to the wires being used in real life

References

[1] V. Mishra and A. Kiourti, "Wrap-Around Wearable Coils for Seamless Monitoring of Joint Flexion," in IEEE

[2] V. Mishra and A. Kiourti, "Wearable Electrically Small Loop Antennas for Monitoring Joint Flexion and Rotation," in IEEE Transactions on Antennas and Propagation, vol. 68, no. 1, pp. 134-141, Jan. 2020, doi: 10.1109/TAP.2019.2935147

[3] E. E. Stone and M. Skubic, “Unobtrusive, continuous, in-home gait measurement using the Microsoft Kinect,” IEEE Trans. Biomed. Eng., vol. 60, no. 10, pp. 2925–2932, Oct. 2013.

[4] F. Ferryanto and M. Nakashima, “Development of a markerless optical motion capture system for daily use of training in swimming,” Sports Eng., vol. 20, no. 1, pp. 63–72, Mar. 2017.

[5] M. El-Gohary and J. McNames, “Shoulder and elbow joint angle tracking with inertial sensors,” IEEE Trans. Biomed. Eng., vol. 59, no. 9, pp. 2635–2641, Sep. 2012.

[6] F. A. de Magalhaes, G. Vannozzi, G. Gatta, and S. Fantozzi, “Wearable inertial sensors in swimming motion analysis: A systematic review,” J. Sports Sci., vol. 33, no. 7, pp. 732–745, 2015.

[7] B. Mariani, M. C. Jiménez, F. J. G. Vingerhoets, and K. Aminian, “Onshoe wearable sensors for gait and turning assessment of patients with Parkinson’s disease,” IEEE Trans. Biomed. Eng., vol. 60, no. 1, pp. 155– 158, Jan. 2013.

[8] Y. Qi, C. B. Soh, E. Gunawan, K.-S. Low, and A. Maskooki, “A novel approach to joint flexion/extension angles measurement based on wearable UWB radios,” IEEE J. Biomed. Health Informat., vol. 18, no. 1, pp. 300–308, Jan. 2014.

[9] J. H. M. Bergmann, S. Anastasova-Ivanova, I. Spulber, V. Gulati, P.Georgiou, and A. McGregor, “An attachable clothing sensor system for measuring knee joint angles,” IEEE Sensors J., vol. 13, no. 10, pp. 4090– 4097, Oct. 2013.

[10] G. Moreton, T. Meydan, and P. Williams, “Investigation and characterization of a planar figure-of-eight coil as a curvature sensor,” in Proc. IEEE SENSORS, Glasgow, U.K., Oct./Nov. 2017, pp. 1–3. [10] V. Mishra and A. Kiourti, "Wrap-Around Wearable Coils for Seamless Monitoring of Joint Flexion," in IEEE Transactions on Biomedical Engineering, vol. 66, no. 10, pp. 2753-2760, Oct. 2019, doi: 10.1109/TBME.2019.2895293.

[11] T. E. Hewett, S. L. Di Stasi, and G. D. Myer, “Current concepts for injury prevention in athletes after Anterior Cruciate Ligament Reconstruction,” *The American Journal of Sports Medicine*, vol. 41, no. 1, pp. 216–224, 2012.

[12] B. D. Roewer, S. L. Di Stasi, and L. Snyder-Mackler, “Quadriceps strength and weight acceptance strategies continue to improve two years after Anterior Cruciate Ligament Reconstruction,” *Journal of Biomechanics*, vol. 44, no. 10, pp. 1948–1953, 2011.

[13] D. Adams, D. Logerstedt, A. Hunter-Giordano, M. J. Axe, and L. Snyder-Mackler, “Current concepts for Anterior Cruciate Ligament Reconstruction: A criterion-based rehabilitation

progression," *Journal of Orthopaedic & Sports Physical Therapy*, vol. 42, no. 7, pp. 601–614, 2012.

[14] S. Di Stasi, G. D. Myer, and T. E. Hewett, "Neuromuscular training to target deficits associated with second anterior cruciate ligament injury," *Journal of Orthopaedic & Sports Physical Therapy*, vol. 43, no. 11, 2013.

[15] C. A. DiCesare, N. A. Bates, K. D. Barber Foss, S. M. Thomas, S. C. Wordeman, D. Sugimoto, B. D. Roewer, J. M. Medina McKeon, S. Di Stasi, B. W. Noehren, K. R. Ford, A. W. Kiefer, T. E. Hewett, and G. D. Myer, "Reliability of 3-dimensional measures of single-leg cross drop landing across 3 different institutions," *Orthopaedic Journal of Sports Medicine*, vol. 3, no. 12, p. 232596711561790, 2015.

[16] "Mesh Generation Overview," *Mesh generation overview*, 2020. [Online]. Available: https://space.mit.edu/RADIO/CST_online/mergedProjects/3D/common_overview/mesh_generation_overview.htm. [Accessed: 09-Dec-2021].

[17] *Biological Data*, 2020. [Online]. Available: https://space.mit.edu/RADIO/CST_online/mergedProjects/3D/common_tools/common_tools_biomodels.htm#Voxel_Family. [Accessed: 09-Dec-2021].

Appendix A: Tutorial on Using CST Posable BioModels

Posable Models

CST BioModels were used during simulations for the proposed models. Specifically, the Posable BioModels models were used in the research. The posable models provide capabilities to change flexion angles before importing the Voxel BioModels. Further details and instructions will be shown in this section using the BioModel Laura who is a s based on a 43-year-old female who is 163 cm and 51 kg [17]. The process for posing the models is the same for all Posable BioModels.

To import Voxel BioModels, first go to home Modeling --> Import/Export --> 3D Files (the one under the Import heading) --> Voxel Data--> Posable Human --> Laura (or any other model you want to use that is available). This will open up CST Human Model Poser, and will look like Figure 16.

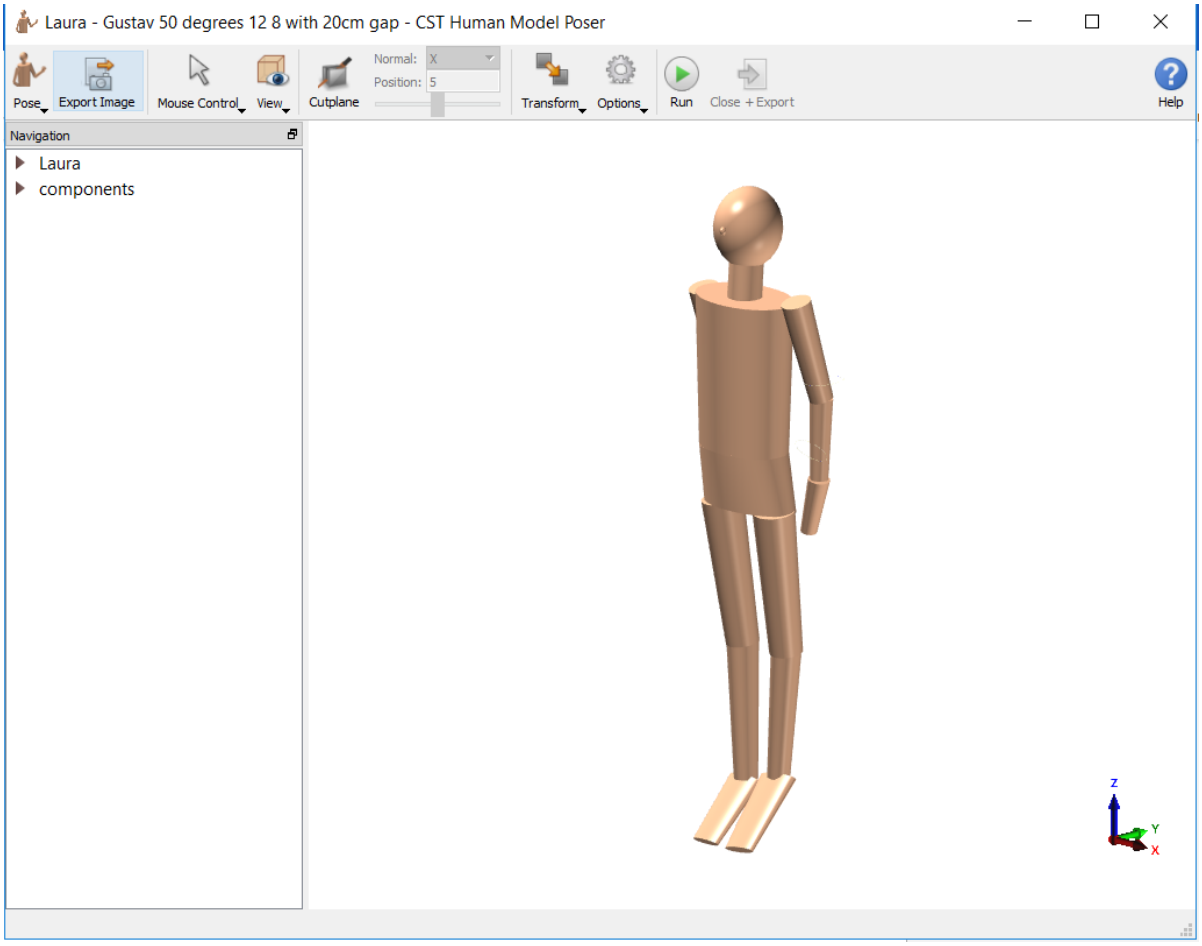

Figure 17: CST Human Model Poser (Laura)

Then you will click on Laura and a drop down menu that looks like Figure 17 will appear.

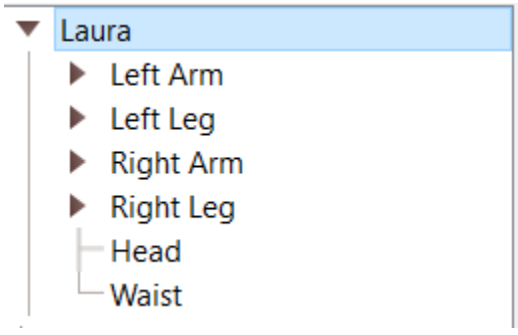

Figure 18: CST Human Model Poser Drop Down Menu (Laura)

There are limitations for flexion and rotation angles. In the following table, all of the ranges of angles for each direction for each part of the limb is shown. In the simulations ran for this research, Left Arm was adjusted. The Upper and Lower parts were adjusted to get the arm to bend at the desired flexion angle and to get the arm to fit inside the coils. Specifically Left Arm Lower in the U direction controls the flexion angle of the elbow.

Table 4: Angle Ranges for CST Human Model Poser

Body Parts	Part of the Body Part	Direction	Angle Range (degrees)
Left Arm and Right Arm	Hand	U	-30 to 30
		V	-70 to 70
		W	0 to 0
	Lower	U	-140 to 0
		V	-45 to 45
		W	-90 to 90
	Upper	U	-150 to 90
		V	-90 to 90
		W	-90 to 90
Left Leg and Right Leg	Foot	U	-90 to 90
		V	-90 to 90
		W	-60 to 60
	Lower	U	0 to 90
		V	0 to 0
		W	0 to 0
	Upper	U	-90 to 90
		V	-90 to 90
		W	-90 to 90
Head	N/A	U	-45 to 45
		V	-45 to 45
		W	-45 to 45
Waist	N/A	U	-45 to 90
		V	-45 to 45
		W	-60 to 60